2021

On the Measurements of Individual Particle Properties Via Compression and Crushing

Chunlong Liu

Fengyin Liu

Jinliang Song

Fuli Ma

Dongfang Wang

See next page for additional authors

Authors
Chunlong Liu, Fengyin Liu, Jinliang Song, Fuli Ma, Dongfang Wang, and Guoping Zhang

Journal of Rock Mechanics and Geotechnical Engineering 13 (2021) 377–389

Contents lists available at ScienceDirect

Journal of Rock Mechanics and Geotechnical Engineering

journal homepage: www.jrmge.cn

Full Length Article

On the measurements of individual particle properties via compression and crushing

Chunlong Liu [a,b], Fengyin Liu [a], Jinliang Song [b,c], Fuli Ma [b,d], Dongfang Wang [b], Guoping Zhang [b,*]

[a] Institute of Geotechnical Engineering, Xi'an University of Technology, Xi'an, 710048, China
[b] Department of Civil and Environmental Engineering, University of Massachusetts Amherst, Amherst, MA, 01003, USA
[c] State Key Laboratory of Geomechanics and Geotechnical Engineering, Institute of Rock and Soil Mechanics, Chinese Academy of Sciences, Wuhan, 430071, China
[d] College of Architecture and Civil Engineering, Taiyuan University of Technology, Taiyuan, 030024, China

ARTICLE INFO

Article history:
Received 16 March 2020
Received in revised form
19 May 2020
Accepted 21 June 2020
Available online 8 October 2020

Keywords:
Elasticity
Hertz contact
Particle crushing
Strength
Yielding
Weibull distribution

ABSTRACT

An experimental study is presented to measure the elastic, yielding, and crushing properties of individual particles under compression using substrates made of aluminum alloy, stainless steel, and sapphire. Carefully selected, highly spherical individual Ottawa sand particles of 0.75–1.1 mm in nominal diameter were compressed between two smooth substrates, and the load–deformation curves were analyzed by Hertz elastic contact theory to derive their reduced modulus and Young's modulus as well as yielding and crushing strengths, which vary significantly with the type of substrate materials. Further analysis of the yielding and plastic deformation at the particle-substrate contact shows that the yield strength or hardness of the substrate materials dominates the local contact behavior and hence affects the measured apparent yielding and crushing strengths. The two softer substrates (aluminum alloy and stainless steel) actually lead to underestimated apparent shear yield strengths of quartz particles by 60.4% and 54.2%, respectively, which are actually the yielding of substrates, while the true particle yielding occurs in the sapphire-particle contact. Moreover, the two softer substrates cause much overestimated crushing strengths of the quartz particles by 50.4% and 36.4%, respectively. Selection of inappropriate substrate materials and inappropriate interpretation of the particle-substrate contact can lead to significant errors in the measured yielding and crushing strengths. It is recommended that single particle compression testing uses substrates with yield strength greater than that of the tested particles and result interpretation also considers the elastic and yielding behaviors of the substrates.

1. Introduction

Significant advances in the micromechanics of granular materials such as sands and other crushable particles have been achieved over the past few decades, which have generated much new knowledge and improved understanding of the behavior of granular materials at the microscale or particle level (Antonyuk et al., 2005, 2010; Rahmanian et al., 2009; Hibare et al., 2011; Peng et al., 2014; Druckrey et al., 2016; Pejchal et al., 2017). In fact, the development of micromechanics has been spurred and facilitated by two major scientific and technological advancements: discrete element method (DEM)-based numerical simulations that deal explicitly with the particle-to-particle interactions (e.g. interparticle contact forces, and particle crushing) at the microscale, and experimental measurements of individual particles' properties such as crushing behavior (particularly particle crushing strength) used as necessary input parameters (e.g. the bonding strength for adhering together numerous small rigid spheres to make up a large agglomerate modeled as a large "parent particle") for DEM simulations. As such, obtaining highly accurate mechanical properties (e.g. crushing strength, elastic modulus, and possible yield strength) of individual particles as input parameters plays a key role in DEM simulations as well as in understanding and prediction of stress–strain-strength behaviors of granular materials. Actually, one limitation of the DEM simulations is the omission or exclusion of purely plastic yielding

* Corresponding author.
E-mail addresses: zhangg@umass.edu, gzhang@alum.mit.edu (G. Zhang).
Peer review under responsibility of Institute of Rock and Soil Mechanics, Chinese Academy of Sciences.

https://doi.org/10.1016/j.jrmge.2020.06.009

phenomenon in the load–deformation behavior of individual particles, although particle crushing is explicitly considered by the adoption of aforementioned "parent particle" concept. Moreover, the particle-to-particle contact stiffness used in most DEM simulations is an averaged parameter derived via inverse analysis from the overall mechanical response of a particle assemblage, but not directly measured from particle contact experiments. These two limitations of DEM simulations make it worthy to further study the elastic and yielding behaviors of individual particles of interest, in addition to crushing strength.

On the other hand, the crushing behavior of sand particles and its pertinent role in the micromechanics of soils and other granular materials have also been extensively studied in recent years. To date, it is widely recognized that particle crushing is a microscopic mechanism governing a wide range of macroscale deformation and strength characteristics of granular materials. First, particle crushing contributes to the one-dimensional (1D) compression behavior, particularly at high stresses (Zhang et al., 1990; Chuhan et al., 2003; Chester et al., 2004; Wu et al., 2004; Brzesowsky et al., 2011). In fact, it is agreed that, during 1D compression of granular materials such as sand, the yielding marks the onset of particle crushing and the macroscopic yielding stress of a sand assemblage is closely related to the single particle crushing strength (McDowell and Harireche, 2002; Cil and Alshibli, 2012; Yoshimoto et al., 2012), while the normal compression (i.e. the post-yielding deformation) is mainly due to the particle crushing (McDowell et al., 1996; Cil and Alshibli, 2012). A similar concept is the "limiting compression curve (LCC)" defined in one of the most rational and sophisticated models, the "MIT-S1" model (Pestana and Whittle, 1995). This concept actually attributes the normal compression deformation, particularly at high stresses, to particle crushing that dominates the deformation behavior, including volume change characteristics. Second, due to particle crushing, a sand assemblage or other granular material can experience continuous deformation under high stresses, resulting in the conversion from a coarse-grained material into a fine-grained one accompanied by significant changes in the material's particle size distribution. In other words, the volumetric change of a sand under high stresses originates from primarily particle crushing and secondarily particle rearrangement to new positions (Santamarina and Cho, 2004; Müller et al., 2013; Pejchal et al., 2017; Todisco et al., 2017). Finally, numerous experimental and microstructural investigations have indicated that the brittle crushing strength is an important parameter controlling the compaction behavior of sand at high stresses (Bagherzadeh et al., 2011; Cil and Alshibli, 2012, 2014; Druckrey et al., 2016). As particle crushing changes the particle size distribution of a brittle particulate material such as sand, it directly affects the mechanical properties, such as the dilation or contraction behavior and internal angle of friction at high stresses (Bolton, 1986).

Classical soil plasticity models cannot describe well the constitutive behavior of granular materials, due to their incapability of considering particle crushing. To date, advances in continuum-based breakage mechanics such as the MIT-S1 model (Cheng et al., 2007) as well as others (Einav, 2007a, b) have enabled the incorporation of particle breakage into the constitutive models. Inspired by the idea of a scalar breakage index, other elastoplasticity models have also been proposed for crushable granular materials (e.g. Daouadji and Hicher, 2010; Kikumoto et al., 2010). In fact, this is different from the treatment of classical soil plasticity models where the plastic deformation of granular materials was modeled within the framework of frictional energy dissipation and hardening plasticity (Roscoe et al., 1958; Roscoe and Burland, 1968). With regard to the microscale failure modes, prior petrographic studies have revealed that the dominant particle failure mechanisms leading to single particle crushing and particle assemblage compaction are the development of intra-particle and trans-particle tensile cracks at the particle contacts resulting from point loading (Chuhan et al., 2002; Chester et al., 2004). Numerically, single particle crushing has been studied using DEM simulations (McDowell and Harireche, 2002; Cheng et al., 2003; Cil and Alshibli, 2012) and fractal theory (McDowell et al., 1996). Wang et al. (2015) examined the statistics of single particle crushing strengths using fractal theory and developed theoretical formula for particle crushing strength by considering the characteristics of crushed particle size distributions and evaluating particle crushability. Kwag et al. (1999) carried out a series of single particle compression tests and discussed in detail the crushing mechanisms of three kinds of particles with different shapes. A representative particle crushing stress which reflects the single particle strength was found to correlate well with the crushability. Lee (1992) examined the crushing strengths of limestones from different geographical origins and found that the crushing strength of a single particle generally increases with decreasing particle size (Chuhan et al., 2002; McDowell and Harireche, 2002), which is in accordance with the observation that, with increasing particle size and hence the number of microstructural defects, the particle becomes weaker (Zhang et al., 1990; Karner et al., 2005).

More recently, naturally occurring sands (e.g. Ottawa sand) and artificially manufactured ceramic, sand-sized particles have been widely used as proppants added to hydraulic fracturing fluids to facilitate and enhance the recovery of oil and gas from tight reservoir formations such as shales and even sandstones (Nakata et al., 2001; Cheshomi et al., 2015; Haki et al., 2017; Du et al., 2018). Knowledge of the mechanical properties (e.g. crushing strength, yield strength, and elastic modulus) of these highly spherical proppants is of key importance for their performance under high geostatic compressive stresses in deep Earth. After being hydraulically injected with fracturing fluids into the fractures of the rocks, proppant particles are subjected to compression loading and may experience elastic and plastic deformations and even crushing. Traditionally, although numerous experiments have been conducted to study the crushing strength of individual particles, the elastic and yielding behaviors of individual particles are less well understood. In fact, as pointed out earlier, the DEM-based micromechanics of sands have failed to explicitly incorporate plastic yielding in numerical simulations, even though particle stiffness and crushing are considered in the particle contact models.

In summary, the mechanical properties of individual particles are of significant importance for the micromechanics of sands and other granular materials as well as the performance of proppants injected into the fractures of rocks, and experimental measurements are usually required to obtain their mechanical properties. This paper aims to evaluate how the varied properties of substrates used in the tests affect the measurements of elastic, yielding, and crushing behaviors of individual particles via single particle compression and crushing testing. To facilitate the analysis and interpretation of experimental results, highly pure and highly spherical Ottawa quartz sand was chosen as the representative granular material studied, together with three different types of substrate materials, i.e. aluminum alloy, stainless steel, and sapphire. It is expected that such a study can shed light upon the accurate measurements of individual particles' mechanical properties and the prudent assessment of previously published data in the literature on individual particles' elastic, yielding, and crushing behaviors, some of which have been widely used as required input parameters in DEM-based numerical simulations.

2. Materials and methods

2.1. Materials

The standard American Society for Testing and Materials (ASTM) 20/30 (i.e. the sand particles can pass the #20 but retain on the #30 sieve meshes) Ottawa silica sand (US Silica Company, Ottawa, Illinois, USA) was used in this study. It occurs naturally as round or spherical particles and consists exclusively of pure quartz minerals with a Mohs scale harness of 7. Only those highly spherical particles, as observed under an optical microscope, were carefully selected for testing (Fig. 1a). Each selected particle was also imaged by the optical microscope (Fig. 1b), and its maximal and minimal diameters, designated as D_{max} and D_{min}, respectively, were then carefully measured with the circumscribing and inscribing circles to the particle's outer boundary. The average of these two measurements, D_{max} and D_{min}, was reported as the nominal diameter (D) of each particle studied.

Three different pairs of highly-polished, flat substrates made of aluminum alloy, stainless steel, and single-crystal sapphire (Ted Pella, Inc., Redding, California, USA) with the Mohs scale hardness of 2.5–3, 5.5–6.3 and 9, respectively, were used for particle crushing testing (Table 1 and Fig. 2). While the two aluminum alloy and two stainless steel substrates were thick and bulky, with a thickness of greater than 2 cm, the two sapphire substrates were thin plates with dimensions of 1 cm × 1 cm × 0.2 cm. Therefore, each of the sapphire substrates was glued to a bulky stainless steel cylinder that was preheated on a hotplate surface to 130 °C using a high-strength thermoplastic mounting adhesive, CrystalBond 509 (Aremco Products, Inc., USA), with a flow or melting point of 121 °C or 250 °F (Fig. 2c), resulting in a composite substrate. Nevertheless, the tested sand particle was in direct contact with

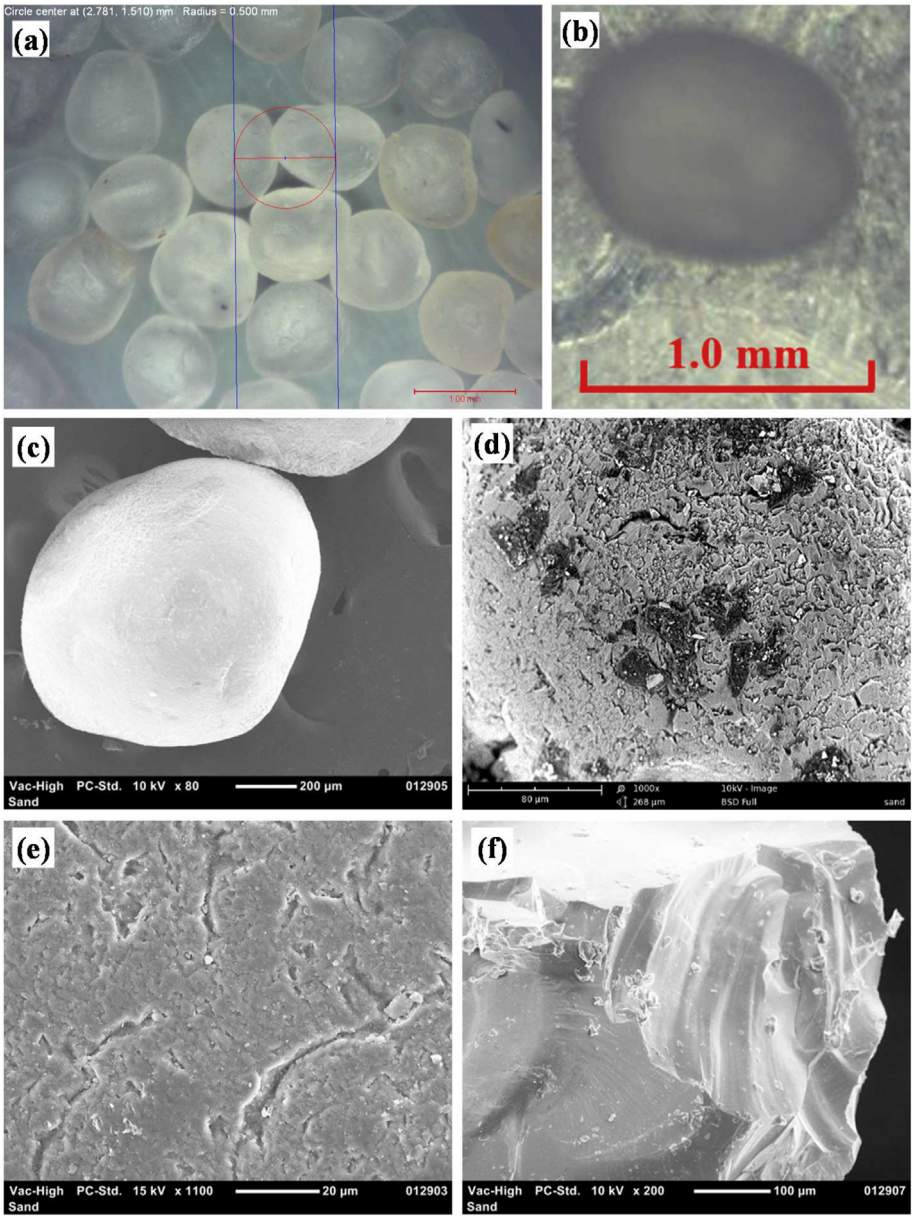

Fig. 1. The natural Ottawa sand particles studied: (a) An optical micrograph showing the geometry and transparency; (b) A nearly spherical particle; (c) A scanning electron microscopy (SEM) micrograph showing a particle's geometry and rough surface; (d, e) SEM micrographs showing the details of surface roughness; and (f) An SEM micrograph showing the smooth fractured surfaces with sharp edges.

Table 1
Basic mechanical properties of the substrate materials.

Material	Mohs scale hardness, H	Young's modulus, E (GPa)	Poisson's ratio, ν	Tensile yielding strength, σ_y (MPa)
Aluminum alloy[a]	2.5–3	70	0.34	386
Stainless steel[b]	5.5–6.3	210	0.29	615
Sapphire	9	379	0.28	–

[a] 7075 aluminum alloy.
[b] AISI type 304 stainless steel.

the hard sapphire, but not the stainless steel cylinder. Some basic mechanical properties of these substrate materials are summarized in Table 1.

2.2. Compression of individual particles

Particle compression tests were performed by placing a selected spherical sand particle between two highly-polished substrates made of the same material (i.e. aluminum alloy, stainless steel, or sapphire) in an automated GeoJac loading frame (Trautwein Soil Testing Equipment, Inc., USA) with a maximum loading capacity of 220 N and a load resolution of 0.1 N (Fig. 2a). Load was monotonically increased at a constant displacement rate of 0.01 mm/min until the particle was broken or crushed, as indicated by a sharp dramatic drop in the load–deformation curve that was continuously monitored during the entire loading process. For each pair of substrates made of the same material, a group of more than 20 particles was tested to obtain statistically meaningful averages of the individual measurements on a single particle to account for the size variability and other heterogeneity (e.g. shape or geometry, surface roughness) of individual sand particles, and hence a total of more than 60 particles was tested for the three pairs of substrates.

Because of the high sphericity of the tested particles, their load–deformation curves were analyzed using the Hertz elastic contact theory that deals with the contact between an elastic sphere and an elastic flat half-space. For a smooth contact between two elastic

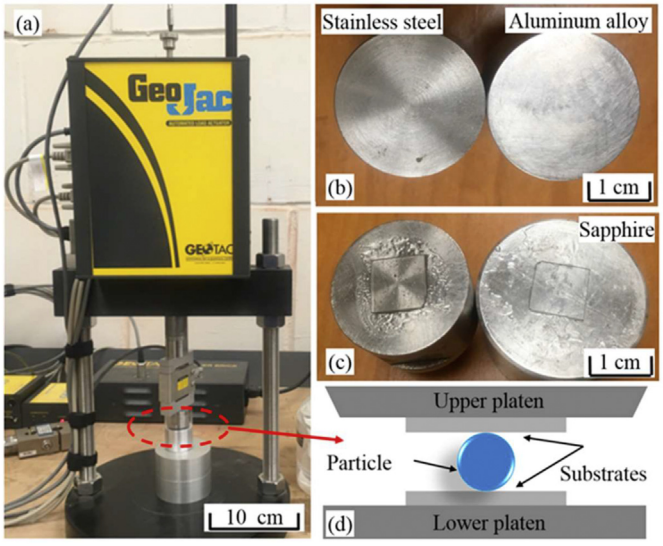

Fig. 2. Experimental setup for single particle crushing testing: (a) The GeoJac loading frame; (b) The stainless steel and aluminum alloy substrates; (c) The thin sapphire plates glued onto the surface of a stainless steel surface used as composite substrates; and (d) Schematic illustration of the contact between a spherical particle and substrates.

bodies such as the quartz particle and substrate, the reduced modulus E_r of the particle-substrate contact can be obtained by fitting the initial elastic response of the experimental load–deformation curve with the following equation developed for a Hertz elastic contact between a sphere and a flat surface (Johnson, 1985; Zhang et al., 2013):

$$E_r = \frac{3P}{(Dd^3)^{1/2}} \tag{1}$$

where P is the load applied on the particle in the elastic regime, and d is half of the total compressive deformation (because of two symmetrical particle-substrate contacts of a particle compressed between two flat substrates). In fact, E_r is the initial linear slope of the Hertz elastic contact line in the compression curve plotted by $3P/D^{1/2}$ versus $d^{3/2}$.

On the other hand, the reduced modulus E_r of the contact between a spherical particle and the flat substrate is given as (Johnson, 1985; Pharr et al., 1992; Fischer-Cripps, 2011; Müller et al., 2011; Zhang et al., 2013; Song et al., 2017, 2018):

$$\frac{1}{E_r} = \frac{1-\nu_1^2}{E_1} + \frac{1-\nu_2^2}{E_2} \tag{2}$$

where E_1 and E_2 are the Young's moduli of the particle and substrate, respectively; and ν_1 and ν_2 are their corresponding Poisson's ratios. Prior work demonstrates that the errors in the assumed Poisson's ratio for the tested material (i.e. quartz particle in this paper) have little or no significant influence on the calculation of its Young's modulus (Menčík and Swain, 1997). Therefore, a constant Poisson's ratio of 0.3 is assumed for all tested Ottawa sand particles.

Through the above curve fitting, the yielding of the particle-substrate contact can also be evaluated. The point where the experimental load–deformation curve deviates from the theoretical Hertz elastic contact line marks the onset of plastic yielding, which can be used to determine the yielding load P_y. Thus, using Tresca's yielding criterion, the shear yield strength τ_y of the contact is computed as (Antonyuk et al., 2005; Zhang et al., 2013):

$$\tau_y = 0.31 p_{max} = 0.31\left(\frac{24 P_y E_r^2}{\pi^3 D^2}\right)^{1/3} \tag{3}$$

where p_{max} is the maximum contact pressure at the onset of plastic yielding, and P_y is the load at which the first yielding takes place near the contact interface. It is noteworthy that the first yielding can occur in either the sand particle or the substrates, depending on their respective yield strength or hardness. Nevertheless, the above equation is used to calculate the shear yield strength of either of the two contact objects.

Because of their high sphericity, the nominal crushing strength, σ_f, of quartz particles is defined by the following equation (Hiramatsu and Oka, 1966; Jaeger, 1967; Shipway and Hutchings, 1993a, b; Luscher et al., 2007; Cavarretta et al., 2010, 2012):

$$\sigma_f = \frac{0.9 P_{max}}{D^2} \tag{4}$$

where P_{max} is the peak or failure load of the entire compressive loading process. In fact, the determination of nominal crushing strength of sand particles has always been controversial. Therefore, the above equation includes a correction coefficient of 0.9 to account for the effects of imperfect particle geometry and surface roughness.

2.3. Statistical analysis

To account for the variability of the three kinds of mechanical properties (i.e. Young's modulus, shear yield strength, and crushing

strength) caused by both intrinsic crystal defects and geometry (e.g. size and shape) of the tested quartz particles, the experimental data (i.e. mechanical properties) obtained by the aforementioned compression testing were further analyzed to obtain the averages using two different statistical approaches for the purpose of comparison: simple arithmetic average and Weibull statistical mean. For the latter, a random variable x, such as the Young's modulus, yield strength, or crushing strength of individual sand particles, is described by the Weibull law, with its cumulative distribution function (CDF) as (Weibull, 1951; Zhang et al., 2013):

$$F(x;\lambda,k) = 1 - \exp\left[-(x/\lambda)^k\right] \tag{5}$$

where $x \geq 0$ is a random variable; $k > 0$ is the shape parameter or, for the distribution of material strength, the Weibull modulus; and $\lambda > 0$ is the scale parameter or nominal value x_0. In general, k can be used to describe the variability of the measured material properties (e.g. strength of brittle materials). It is typically considered as a measurement of the distribution of physical flaws (e.g. crystal defects, joints in rocks, or dislocations) or weak links in a material (Jayatilaka and Trustrum, 1977; Danzer et al., 2007). A larger k value indicates that the flaws are more evenly distributed, and hence the material behaves more uniformly, and its properties are less scattered. On the other hand, if flaws are grouped or associated non-evenly or non-uniformly, the material exhibits highly variable properties. As such, the resulting k value is relatively small.

The statistical mean or characteristic value of the Weibull variable X is

$$E(X) = \lambda\Gamma\left(1+\frac{1}{k}\right) \tag{6}$$

where Γ is the gamma function.

The variance of the Weibull variable X is

$$var(X) = \lambda^2\left\{\Gamma\left(1+\frac{2}{k}\right) - \left[\Gamma\left(1+\frac{1}{k}\right)\right]^2\right\} \tag{7}$$

This equation indicates that the mean value of the Weibull variable X depends on both k and $\lambda = x_0$, with the former expressed through the gamma function.

Eq. (5) can be re-arranged into

$$\ln\{-\ln[1-F(x)]\} = k\ln(x/\lambda) = k\ln(x/x_0) \tag{8}$$

Thus, by fitting the experimental data points plotted by $\ln\{-\ln[1-F(x)]\}$ vs. $\ln(x/x_0)$ with a straight line, its slope is the value of k. The nominal value x_0 corresponds to a failure probability of 63.2% or a survival probability of 36.8%. The survival probability F of the particles is determined by the median rank method:

$$F_i = \frac{i-0.3}{n+0.4} \tag{9}$$

where n is the total number of data points, and i is the rank of the considered data point.

In the subsequent analyses, four different parameters, including the reduced modulus E_r, Young's modulus of sand particles E, yield strength of the contact interface τ_y, and particle crushing strength σ_f, are considered as Weibull random variables and hence are discussed in the replacement of a general variable x.

2.4. Surface characterization

Examination of particle surfaces was conducted in a Zeiss Evo 50 scanning electron microscopy (SEM) (Cambridge, UK) operated at 15 kV and 100 μA. Both original sand particle and selected particle fragments from crushing testing were observed to compare the surface features. A thin layer of conductive carbon coating of ~12 nm in thickness was applied on the examined particles in an Edwards AUTO 306 vacuum coater (Edwards Company, Burgess Hill, UK) before SEM scanning. Micrographs were acquired using both secondary electron (SE) and backscattered electron (BSE) signals.

3. Analysis of results

3.1. Extraction of mechanical properties

As expected, the size of more than 60 tested particles selected from the ASTM 20/30 silica sand varies slightly. The nominal diameter (D) of all tested particles ranges from 0.75 mm to 1.1 mm. Table 2 summarizes the size and shape of all studied particles sub-grouped by three different substrates. While the nominal diameter D of each sub-grouped particles are 0.845 mm, 0.887 mm, and 0.932 mm for aluminum alloy, stainless steel, and sapphire substrates, respectively, and the shape of these particles is described by three different parameters, including $D_{max} - D_{min}$, $(D_{max} - D_{min})/D$, and sphericity. The sphericity is defined as the ratio of diameter of the inscribing circle (i.e. D_{min}) to that of the circumscribing circle (i.e. D_{max}). The inscribing and circumscribing circles' radii are the shortest and longest distances from the contour of the particle to its gravity center, respectively. The sphericity of the tested particles ranges from 79.16% to 80.42%, close to a sphere with a sphericity of 1; while the $(D_{max} - D_{min})/D$ values are nearly 21%–23%. Of course, these particles are not ideally spherical, and the effect of their imperfect shape will be discussed later.

Fig. 3 shows some load–deformation curves obtained from the single particle compression testing. Fig. 3a plots the load–deformation curve in the original P-d plots for an arbitrary sand particle to show the curved theoretical Hertz elastic contact line, the yielding point where the Hertz elastic contact line deviates from the experimental measurements, the peak or crushing load P_{max}, and multiple crushing events after the peak load. Fig. 3b illustrates the existence of the linear sections (i.e. the theoretical Hertz elastic contact line) in the load–deformation curves replotted in the transformed axes (Eq. (1)), without showing the post-crushing or post-failure sections, and compares the three elastic contact lines from three different sand particles compressed between three different substrate materials (i.e. aluminum alloy, stainless steel, and sapphire), respectively. It is noteworthy that the three sand particles shown in Fig. 3b have nearly the same diameter, D = 0.85 mm, 0.89 mm and 0.93 mm, respectively, but their elastic contact lines have different slopes. As pointed out earlier, the slopes of the linear lines used to fit the data points in Fig. 3b are the reduced modulus E_r of the particle-substrate contact for three different substrate materials, respectively. In addition, other important features are also observed:

Table 2
Summary of the size and shape of all tested particles for each substrate (each value is represented by an arithmetic mean of one time the standard deviation).

Substrate	Nominal diameter, D (mm)	$D_{max} - D_{min}$ (mm)	$(D_{max} - D_{min})/D$ (%)	Sphericity, D_{min}/D_{max} (%)
Aluminum alloy	0.845 ± 0.053	0.196 ± 0.063	23.21 ± 7.21	79.16 ± 5.76
Stainless steel	0.887 ± 0.057	0.193 ± 0.065	21.82 ± 7.58	80.31 ± 6.32
Sapphire	0.932 ± 0.058	0.202 ± 0.07	21.68 ± 7.96	80.42 ± 5.6

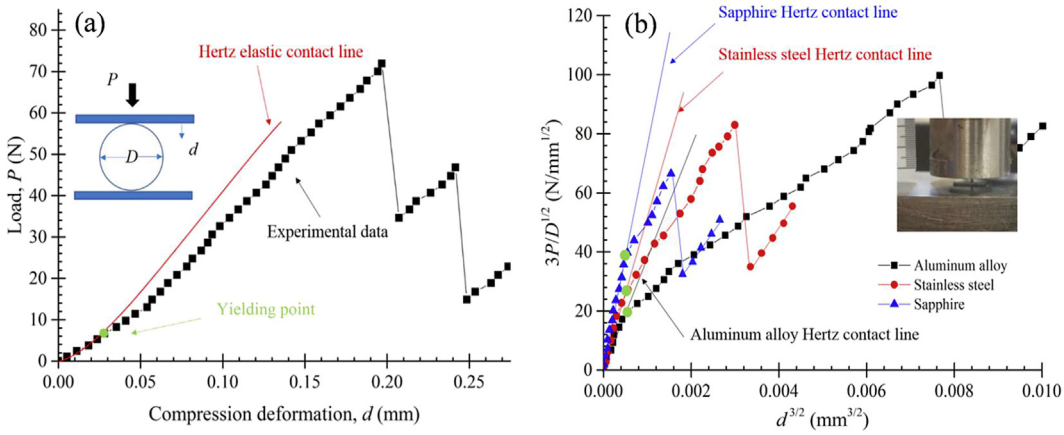

Fig. 3. Load-deformation curves from single particle compression testing: (a) The Hertz elastic contact line in the *P-d* plot (inset shows the test configuration); and (b) Fitting the Hertz elastic contact lines to experimental data plotted in the transformed axes for three different substrates (inset shows the test setup for the sapphire substrates, and part of the post-crushing section is not shown).

(1) Although the tested sand particles are of all quartz mineral, the slope of the Hertz elastic contact line or the reduced modulus of the particle-substrate contact increases from aluminum alloy, to stainless steel, and finally to sapphire substrates, indicating that the measurements are affected by the substrate material.
(2) The yielding load also varies with different substrate materials: sapphire gives the highest yielding load, while the aluminum alloy indicates the lowest one.
(3) The peak failure points are affected by the substrate material as well: the particle crushed between sapphire substrates has a much lower peak load than the one crushed between aluminum alloy ones, while the sand crushed between stainless steel substrates has the intermediate peak load.

To further illustrate the above observations, Fig. 4a–c shows all individual load–deformation curves with transformed axes (Eq. (1)) sub-grouped by different substrates, respectively, together with their averaged load–deformation curves based on the results from 20 particles tested in each substrate. Fig. 4d also compares the averaged load–deformation curves for the three substrate materials. Although certain scattering and dispersion of these load–deformation curves can be observed for each group of 20 particles, the overall trends of the averaged curves shown in Fig. 4d are consistent with those observed in Fig. 3b. While it is redundant to repeat the same features observed in Figs. 4d and 3b, it is prudent to point out that averaging the 20 individual load–deformation curves obtained from each pair of substrates tends to cause the disappearance of a well-defined linear section of the curves represented by the Hertz elastic contact as well as the well-defined yielding point. Therefore, as described in the following section, each individual load–deformation curve, but not the averaged curve, is analyzed to estimate the mechanical properties of the sand particles or the sand-substrate contact.

For each of the 60 tested particles, the reduced modulus E_r, yielding load P_y, and crushing load P_{max} are obtained from its pertinent load–deformation curve. Because of the variations in particle size as well as the randomly-occurring crystal defects in the polycrystalline quartz particles, the crushing strength σ_f varies significantly with the nominal diameter D as well as the substrate material (Fig. 5a). For the tested Ottawa sand particles with sizes ranging from 0.75 mm to 1.1 mm, their crushing strength ranges from ~30 MPa to ~220 MPa, and the results for different substrates are all randomly mixed and scattered (Fig. 5a). In fact, similar phenomena were reported for other silica sands (Lee, 1992; Nakata et al., 2001). In Fig. 5b, the crushing strengths of four different silica sands ranging from ~5 MPa to ~500 MPa (i.e. over a range of two orders of magnitude) are highly scattered, although they generally decrease with the particle size D. Even for one particular type of sand, its crushing strength is also highly scattered. Moreover, the size variation of these sand particles has a much wider range from ~0.1 mm to ~2 mm. For the studied Ottawa sand, the size range is much smaller (i.e. from 0.75 mm to 1.1 mm). Therefore, to differentiate explicitly the effect of different substrate materials on sand crushing testing, statistical analyses of the experimental data are performed, and results are discussed in the next section.

3.2. Statistical analyses

Fig. 6 plots the Weibull distribution of the three measured mechanical properties, including the reduced modulus E_r, the shear yield strength τ_y, and the crushing strength σ_f. For each property, the data are subdivided into three groups according to each specific substrate material. Clearly, all of measured data can be fitted well by a straight line described by Eq. (8). Both the k values (i.e. the slope of the fitting straight line) and coefficient of determination R^2 are included in the plots. The R^2 values are all greater than 0.955, indicating the data's consistency. With regard to the mechanical properties of materials, k is also termed Weibull modulus. All k values are much greater than 1. Moreover, the higher the k value, the lower the variation of the measurements. For example, a higher k value for the shear yield strength obtained with the sapphire substrates indicates a lower variation in the measurement, which can be likely caused by the highly smooth surface (i.e. no scratches or surface contamination) of the single-crystal sapphire substrates, because rough, contaminated surfaces of two contact bodies introduce additional friction or adhesion, making the contact behavior deviate from the idealized Hertz elastic contact (i.e. smooth and non-adhesive contact) theory. Furthermore, using Eq. (6), the Weibull mean values for each group of sand particles tested on a specific substrate can be obtained from these plots, which are further discussed below.

As pointed out earlier, since the tested sand particles fall in a very narrow size range, they can be considered as one particular size group (e.g. ASTM size 20/30). Two different statistical methods,

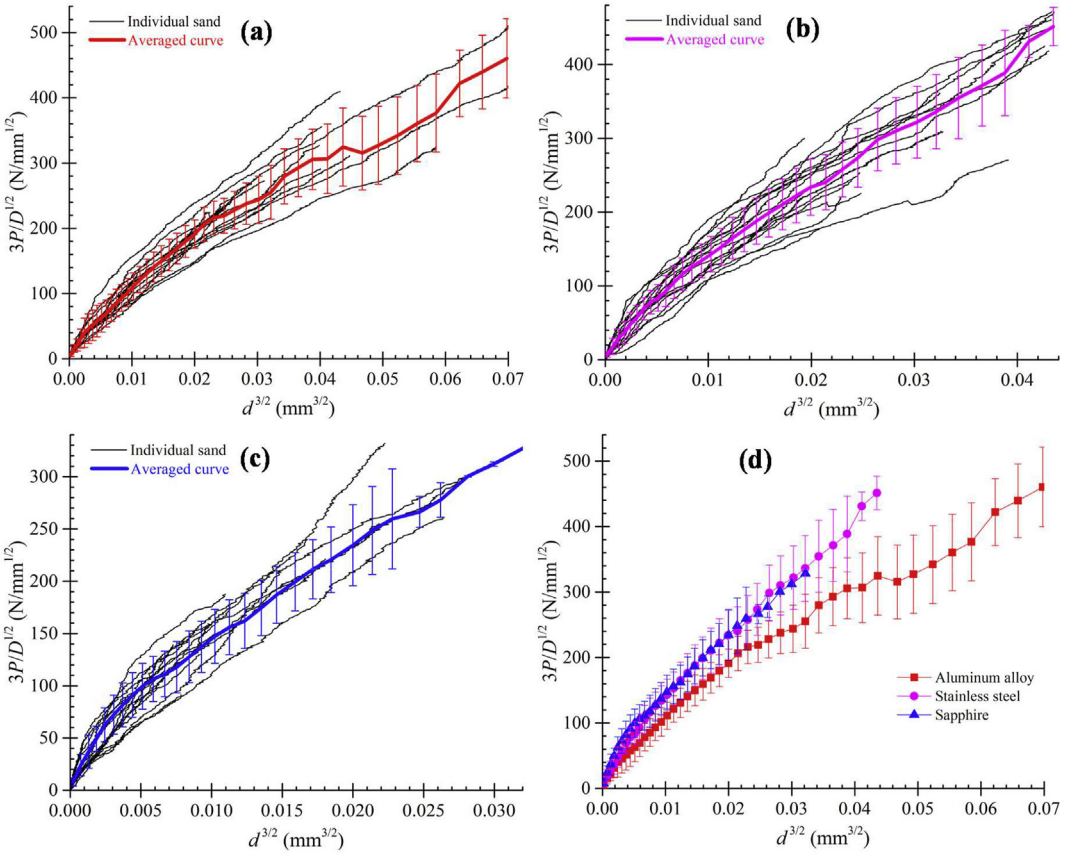

Fig. 4. Individual and averaged load–deformation curves with transformed axes from single particle compression testing: (a) Aluminum alloy substrates; (b) Stainless steel substrates; (c) Sapphire substrates; and (d) Comparison of three averaged curves for three different substrates. All error bars denote one standard deviation.

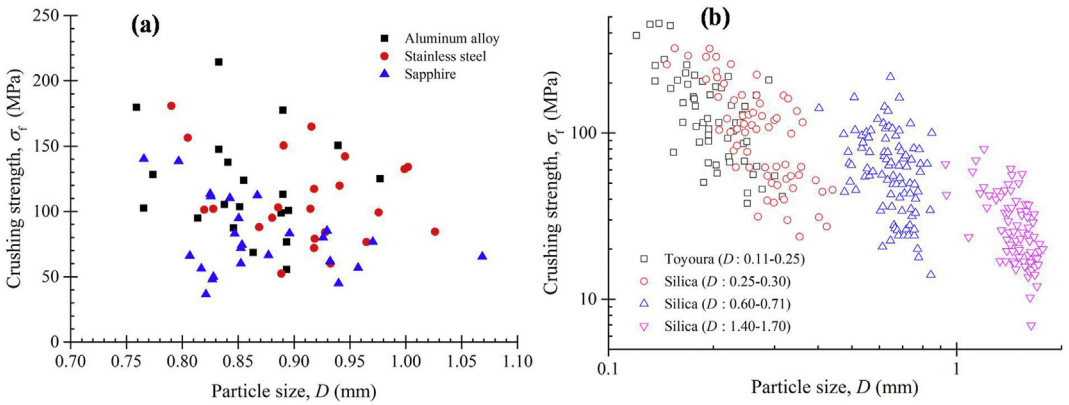

Fig. 5. Variation of particle crushing strength with particle size: (a) The studied Ottawa quartz sand tested by three different substrates; and (b) Some silica sands reported in the literature (after Lee, 1992; Nakata et al., 2001).

including the simple arithmetic mean and Weibull mean, were used to obtain the averages of these mechanical properties. Table 3 summarizes the nominal value (i.e. x_0) and mean value ($E(x)$) of the three mechanical properties, including the reduced modulus, shear yield strength, and crushing strength obtained by Weibull analysis. As expected, all mean values are less than the respective nominal values, which correspond to a failure probability of 63.2%. The mean values also differ with different substrate materials. As discussed later, some of these values are actually the apparent or "false" representation of the true behaviors of the quartz sand particles, depending on the local particle-substrate contact behavior.

3.3. Effects of different substrate materials

Fig. 7 compares the mean values of reduced modulus E_r of the contact, Young's modulus E, shear yield strength τ_y, and crushing strength σ_f of the sand particles obtained from different particle-substrate contacts or based on different substrate materials. In these plots, the two averages (the arithmetic mean and Weibull mean) are also included for comparison. The error bars represent one standard deviation of each respective set of data. Surprisingly, there is no great difference between the two mean values for each specific substrate material, although sometimes the standard

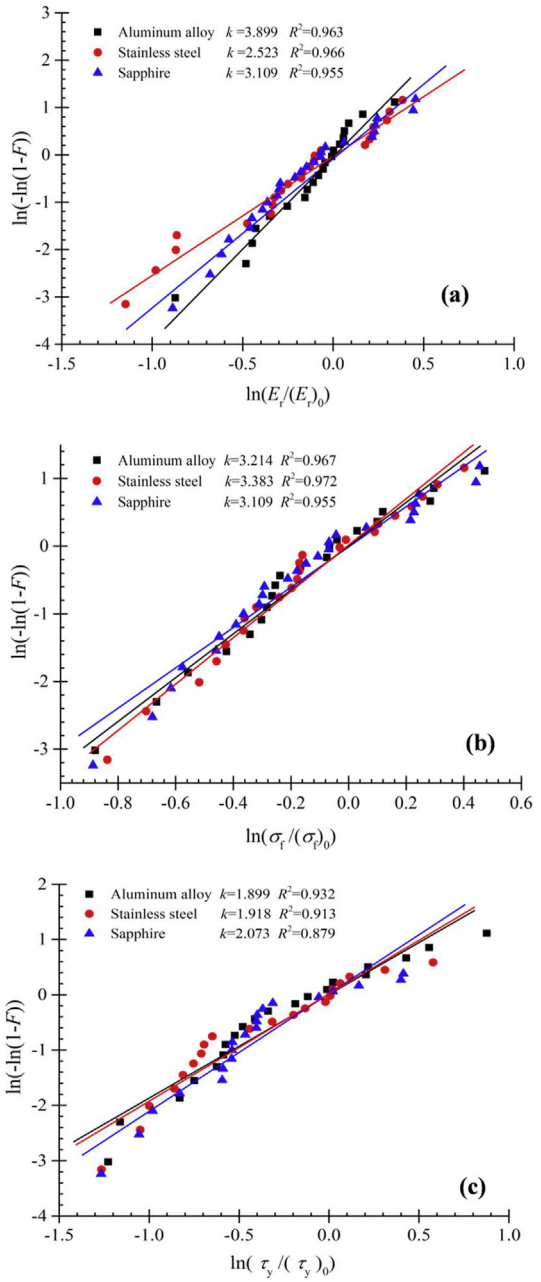

Fig. 6. Weibull distributions of (a) reduced modulus, (b) particle crushing strength, and (c) shear yield strength, subdivided based on different substrate materials.

deviations may vary more significantly. The most likely reason is that the size ranges of the tested particles are very small and hence each subgroup of tested particles can be regarded as one size or a uniform particle group. Otherwise, the two mean values may differ considerably. Therefore, in the subsequent discussion, no effort is made to differentiate the two different mean values, since each set of mean values is nearly the same as the other.

In Fig. 7a, the sapphire substrates obtain the highest reduced modulus, while the aluminum alloy ones have the lowest one, and the reduced modulus obtained from the stainless steel ones is in the middle. This observation concurs with the elastic contact theory described by Eq. (2). If the tested individual Ottawa sand particles have the same Young's modulus, which should be expected, then the reduced modulus E_r of the particle-substrate contacts can be substantially affected by the Young's modulus of the substrate material. This can be verified by the results shown in Fig. 7b where the average Young's modulus of quartz sand calculated from the reduced Young's modulus is nearly the same, around 72–75 GPa. As such, the elastic modulus of the sand particles can be concisely obtained only if the substrate materials' elastic properties (including Young's modulus and Poisson's ratio) are explicitly considered in the particle-substrate contacts. In Fig. 7c, the "apparent" shear yield strength, computed from Eq. (3) based on the compression curves for different substrates, differs significantly from each other. In fact, the aluminum alloy substrates have the lowest apparent shear yield strength, while the sapphire has the highest one. To understand this large discrepancy in the apparent shear yield strength, the particle-substrate contact behaviors for different substrate materials need to be analyzed.

In general, when two objects are brought into contact with each other, initial elastic deformation occurs at small loads, followed by the transition to some local yielding and plastic deformation upon increasing load. Although both objects experience elastic deformation during the entire loading process, yielding and plastic deformation always occurs first in the object with a lower hardness or yield strength. When the load continues to increase, yielding may then occur in the other one with a higher hardness. Unfortunately, identification and assessment of the yielding event occurring in the second harder object are usually difficult, as it is masked by the plastic deformation that has already occurred in the softer one. As shown in Table 1, the Mohs scale hardness values of the three substrate materials, i.e. aluminum alloy, stainless steel, and sapphire, are 2.5–3, 5.5–6.3 and 9, respectively, while quartz has a Mohs scale hardness of 7. Therefore, during the compression of individual quartz particles, occurrence of the first yielding events needs to be assessed in conjunction with the hardness of both the tested material (i.e. quartz sand) and substrates. As shown in Fig. 8a, for aluminum alloy and stainless steel substrates, compression of a quartz particle between two substrates leads to the first yielding occurring in the aluminum alloy or stainless steel substrates, but not in the particle. Upon the occurrence of the first yielding, the experimental load–deformation curve starts to deviate from the theoretical Hertz elastic contact line. However, the first yielding occurs in the quartz particle when sapphire is used as the substrate material (Fig. 8b). Therefore, the apparent shear yield strengths directly interpreted from the load–deformation curves using Eq. (3) do not represent the true yielding of the tested quartz particles. In fact, in Fig. 7c, only sapphire or another material with hardness greater than that of quartz can be used as substrates to

Table 3
Apparent reduced modulus, shear yield strength, and crushing strength obtained from Weibull statistical analyses.

Substrate	Reduced modulus, E_r (GPa)		Shear yield strength, τ_y (MPa)		Crushing strength, σ_f (MPa)	
	Mean	E_{r0}	Mean	$(\tau_y)_0$	Mean	$(\sigma_f)_0$
Aluminum alloy	39.1	38.9	265	267	119.7	133.7
Stainless steel	55.8	56.3	306.7	382	108.6	121
Sapphire	65.9	65.4	669.5	876	79.6	89.1

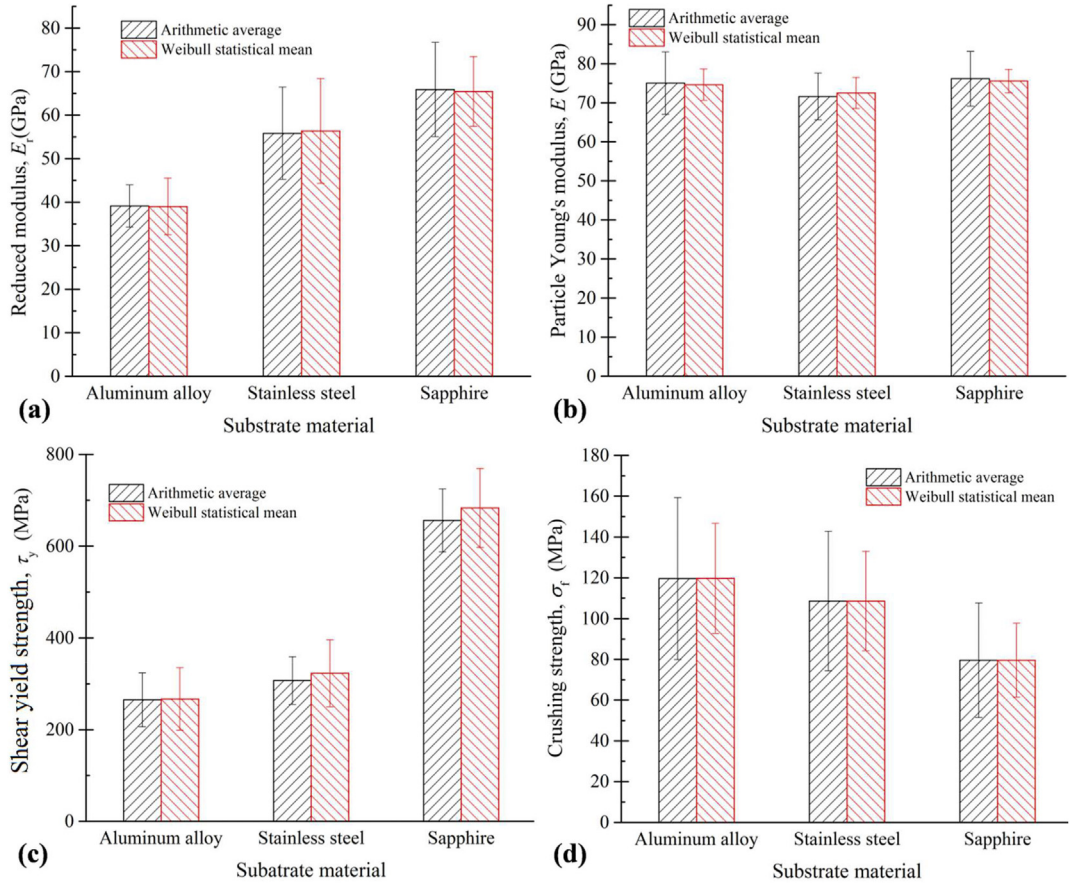

Fig. 7. Weibull statistical mean and arithmetic mean values of (a) reduced modulus, (b) Young's modulus, (c) shear yield strength, and (d) crushing strength.

accurately measure the true shear yield strength of the tested particles in the single particle compression and crushing testing. The apparent shear yield strengths obtained for the two other substrates (i.e. aluminum alloy and stainless steel) are actually the yield strengths of the substrate materials, but not the tested quartz particles. This observation demonstrates the importance of selecting an appropriate material as substrates for particle compression testing. In summary, the shear yield strength obtained for the sapphire substrates is the true yielding occurring in the tested particles. The two softer substrates (aluminum alloy and stainless steel) provide apparent yield strengths of the substrates, which are 60.4% and 54.2% smaller than the actual yield strength of quartz, respectively. It is also interesting to compare the measured apparent shear yield strengths with the true tensile yield strengths of the substrate materials. Table 1 also shows the uniaxial tensile yield strengths (σ_y) of the aluminum alloy and stainless steel. In general, the shear yield strength $\tau_y = (0.5–0.57)\sigma_y$. The measured shear yield strengths of the two softer substrates actually agree well with the uniaxial tensile yield strength, validating that the apparent yielding actually occurs in the two softer substrates (i.e. aluminum alloy and stainless steel).

While yielding of individual sand particles may not be so important in DEM modeling, the crushing strength of individual particles is of great importance for DEM simulation and for understanding and predicting the DEM-simulated mechanical behavior of granular materials. Fig. 7d compares the crushing strength of the sand particles measured for different sets of substrates. An interesting observation is that the trend is opposite to that of the shear yield strength shown in Fig. 7c. The softest aluminum alloy substrates give the highest crushing strength, while the sapphire ones obtain the lowest strength, despite that the tested quartz particles were all randomly selected from the same batch of Ottawa sand sample. In fact, the crushing strengths of the aluminum alloy and stainless steel substrates increase by 50.4% and 36.4%, respectively, when compared with that of sapphire ones. Again, the process of contact deformation needs to be analyzed to further assess the true crushing strength of individual sand particles.

When two objects with different hardness or yield strengths are brought into contact, yielding and plastic deformation will occur first in the one with a lower hardness. In the case of a spherical quartz particle in contact with an aluminum alloy or stainless steel substrate, local yielding occurs first around the contact point in the metal substrates, but not in the quartz particle, because the hardness of aluminum alloy and stainless steel is smaller than that of quartz (Table 1). With increasing load, the local yielding is then followed by indentation or penetration of the quartz particle into the aluminum alloy or stainless steel substrate. As such, once the quartz particle starts to penetrate into the substrate, the contact area increases significantly (i.e. a conversion from point contact to curved surface contact), resulting in certain lateral confinement to the top and bottom parts of the sand particle (Fig. 8a), which are the locations for splitting the particle. Such a lateral confinement acts as a kind of additional lateral stress that can actually increase the level of stress for particle breakage or splitting. When the two sets of softer substrates (aluminum alloy and stainless steel) are compared, certainly the depth of penetration and hence the amount of lateral confinement are higher in the softer aluminum alloy than those in the intermediate stainless steel substrates, and more lateral confinement means higher crushing strength. Therefore, the

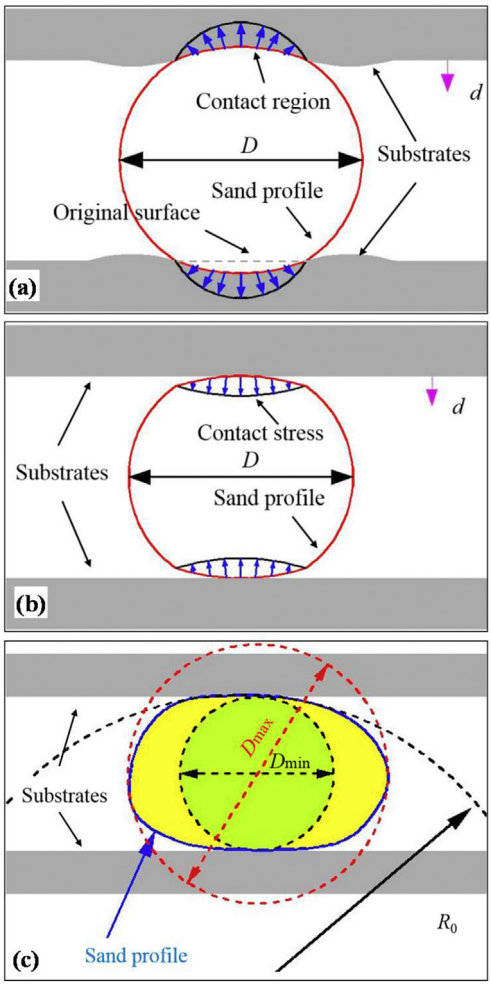

Fig. 8. The local contact behavior for different substrates: (a) Yielding of the softer substrates such as aluminum alloy and stainless steel; (b) Yielding of the particle in sapphire substrates; and (c) Effect of imperfect particle shape.

apparent crushing strength obtained for the aluminum alloy substrates is even higher than that for the stainless steel ones. For sapphire with a hardness even greater than that of quartz, the contact between the quartz particle and sapphire substrate causes quartz particle to first yield locally in the vicinity of contact, but not in the sapphire substrate (Fig. 8b). As such, during compression, no extra lateral confinement is generated and applied to the spherical quartz particle, and the measured crushing strength is actually the true value of the quartz particle. Therefore, sapphire substrates can successfully capture the contact behavior and brittle fracture of Ottawa sand particles. In summary, in individual particle crushing testing, using substrates with hardness lower than that of the tested particles tends to cause extra lateral confinement before particle crushing, and hence overestimates the true crushing strength. Instead, a substrate with the hardness greater than that of the tested particles should be used in individual particle crushing testing.

4. Discussion

4.1. Effects of particle shape and size

The above analysis assumes that the tested particles are ideal spheres. However, as shown in Fig. 1a–c, their shape deviates from ideal spheres to a certain extent. Such imperfect particle shapes are also reflected by the particle dimensions shown in Table 2. As shown in Fig. 8c, an actual quartz particle with the nominal, maximal, and minimal diameters (D, D_{max}, and D_{min}) is being compressed between two flat substrates. Due to the imperfect shape, the actual contact radius R_0 can be different from $D/2$, $D_{max}/2$, or $D_{min}/2$. However, unless the contact occurs between two flat planes (or a flat plane) and a cylindrical surface, the initial contact always starts with a point, and the actual local contact surface of the particle can always be approximated by a part of an ellipsoidal or spherical surface (Johnson, 1985). As such, the imperfect spherical particle shape can definitely affect the measurements of elastic properties, but the degree of influence is limited, due to the very small contact area at the elastic deformation regime. On the other hand, the effect of particle size (D) is explicitly considered in the Hertz elastic contact theory, and the experimental data can be normalized by Eq. (1) to eliminate the absolute effect of particle size.

In general, the elasticity of a material is mainly controlled by the type of atomic bonds, but not too much by crystal defects or their size. Ideal low quartz crystals consist of silica tetrahedra ($[SiO_4]^{4-}$) as the basic units that share the four corner oxygen atoms with an adjoining tetrahedron to form a framework structure. As a naturally occurring material, quartz crystals must contain certain defects such as dislocations, isomorphous substitutions, and joints, among others. However, these crystal defects do not affect the majority of atomic bonds. Therefore, the Young's modulus of quartz sand particles does not vary significantly with their size or shape. Single particle crushing testing definitely involves the use of substrates and hence the particle-substrate contacts. Since the elastic deformation of the particle-substrate contact is usually very small or does not involve local yielding, the reduced modulus of the contact only depends upon the elastic behaviors of the particle and substrates. As shown in Fig. 6b, as long as the elastic properties of the substrates are explicitly considered in the data analysis, the experimentally obtained Young's modulus of the sand particles does not vary too much with the substrate materials, nor their size or shape.

On the other hand, yielding is the onset of plastic deformation, and the plastic behavior of a solid continuum is mainly controlled by dislocations and other microstructural defects or features (e.g. grain boundaries in metals). Defects usually occur in crystal formation or when previously subjected to external mechanical forces. According to previous findings (Nakata et al., 2001; Qian et al., 2019), the larger the sand particle, the more the number of crystal defects. In addition, the size of defects or flaws also increases with particle size. As such, the yield strength of quartz sand particles can vary with particle size or shape, and usually a larger-sized sand particle exhibits lower yield strength. Fortunately, the tested sand particles fall in a very narrow range of sizes, and hence their yield strength may not be highly affected by their size variation. However, as shown in Fig. 8c, the deviation of the particle shape from the ideal spheres may lead to significant errors in the local contact behavior (e.g. overestimated or underestimated contact radius). Therefore, both particle size and shape can affect the accurate measurements of the shear yield strength. For the studied batch of Ottawa sand with nearly a uniform size range, the particle shape may be the dominant factor causing the variations in the shear yield strength.

Finally, similar to the yield strength, the crushing strength of sand particles is significantly affected by particle size, because the larger the particle, the more the defects. Prior work finds that the density of defects increases with particle size (Nakata et al., 2001; Wenzel and Nirschl, 2015). It is well known that the particle crushing strength decreases with increasing particle size (Fig. 9). Moreover, if the particle is not spherical in shape, several early crushing events may take place in relatively small and sharp

angular sections of the particle and hence lower crushing strength may be obtained. On the other hand, a spherical particle with more uniform surface curvature or less angularity may exhibit only one unique crushing event with a higher crushing strength. Therefore, both particle size and shape can significantly affect the particle crushing strength. In fact, such an effect of particle shape is also implicitly considered in the calculation of crushing strength by including a correction factor of 0.9, as shown in Eq. (4).

In summary, particle size does not affect the elasticity of sand particles, but can directly affect the yielding and crushing strengths of the tested quartz sand, owing to the fact that the dimensions and densities of crystal defects within a particle increase with size. With respect to the measurements, the imperfect particle shape may have limited effect on the measured Young's modulus, as the local elastic contact area is usually small. The effect of imperfect particle shape on crushing strength is implicitly considered by a correction factor of 0.9 in the calculation of particle crushing strength. As such, without an appropriate correction method, the yield strength of the particles is more prone to errors caused by the imperfect particle shape.

4.2. Effects of surface roughness and cleanness

The estimation of the particle Young's modulus and yield strength is based on the Hertz elastic contact theory, which assumes clean, smooth, nonconformed contact between two elastic bodies where no friction or adhesion should exist in the contact interface. Surface cleanness or contamination may cause the surfaces to be either rough (such as solid dust microparticles) or adhesive (e.g. greasy finger prints or soft rubbery films). In this case, either friction or adhesion may generate as two contaminated surfaces approach each other into contact. In the preliminary testing of this study, attempts were made to reduce the potential friction by applying a thin layer (e.g. a few micrometers) of vacuum grease coating on substrate surfaces. As a result, although interfacial friction in the contact surfaces was reduced, it was difficult to obtain the initial Hertz elastic contact line in the recorded load–deformation curves as well as the first yielding point, because the first yielding occurred at even very small load or displacement due to the soft nature of the vacuum grease. As such, subsequent testing did not use vacuum grease coating at all, and the interfacial friction was reduced or minimized by highly polishing the substrate surfaces. Nevertheless, as shown in Fig. 1c–e, the tested sand particles do not possess smooth surfaces, and hence the interfacial contact friction may cause overestimation of the particle Young's modulus, shear yield strength, and crushing strength. As such, a general recommendation for single particle crushing testing is that lubricating substrate surfaces should be performed for the crushing strength measurement, but should be avoided if the sand particles' Young's modulus and yield strength are desired.

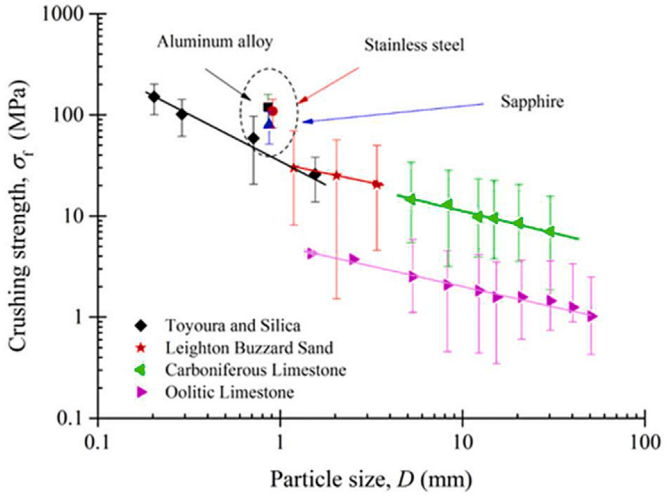

Fig. 9. Effect of particle size on single particle crushing strength. Data are from this study and previous work (Lee, 1992; Nakata et al., 2001).

Careful observations of the surfaces of tested quartz particles under SEM (Fig. 1d and e) found that the surface of the particles is not smooth and the roughness is characterized by flat plateaus, but not by sharp asperities (Fig. 10). The studied Ottawa sand is a naturally occurring material that has undergone extensive and prolonged transport and movement during which interparticle collision and abrasion as well as dissolution take place continuously. As a result, the sharp asperities or angular spikes, if any is presented previously on the surfaces, have been worn away gradually, resulting in a rough surface characterized by relatively flat plateaus separated by narrow and shallow groves (Fig. 1d and e, and 10b). This is in contrast to the smooth surface observed in the crushed sand fragments with sharp, angular edges (Fig. 1f). Although the actual particle surface is far from the ideal smooth surface assumed by the Hertz elastic contact theory (Fig. 10a), the effect of surface roughness on the particle crushing testing is expectedly much smaller than the one with sharp asperities (Fig. 10c). Moreover, friction is a complex concept, and it depends upon the shape and size, as well as the stiffness and yielding of the asperities on the rough surfaces. More accurate assessment of the effect of surface roughness requires more information on surface roughness, actual contact areas (or the ratios of the actual asperity contact area to the projected contact area), and sophisticated contact models. Such a quantitative evaluation is out of the scope of this paper.

Finally, the rough surface may have a more significant effect on the crushing strength. As shown in Fig. 10c, due to stress concentration in the evenly reduced contact area, sharp asperities can easily indent and penetrate into a softer substrate, or crush prematurely when contacting a harder substrate. In either case, the crushing strength is likely to be affected by the surface roughness. Fortunately, the surfaces of the studied Ottawa sand particles do not possess sharp asperities, but are characterized by the relatively flat plateaus. As such, the effect of surface roughness on the crushing strength is limited.

4.3. Comparison with previous data

In the literature, there is a great number of data on the crushing strength of sand particles with a wide variety of mineralogy (e.g. quartz, silica, carbonate, diatom, and alumina). While DEM simulations can yield some of these data, most results were obtained from single particle crushing testing involving compressing individual sand particles between two flat substrates. Because of the irregular shapes of some tested sand particles, few studies tried to evaluate the elastic or yielding behavior. As a result, most studies were reported on the crushing strength. However, some of these studies did not include the details of substrate materials or failed to recognize how the substrate materials affect the accuracy of the measurements. While the importance of local yielding in the vicinity of particle-substrate contact has been noticed in some publications (e.g. hardened steel instead of regular steel was chosen as the substrates for the crushing tests of quartz sands (Yamamuro et al., 1996; Hibare et al., 2011; Pejchal et al., 2017)), effort made to use even harder substrates such as sapphire has not been reported in the literature. Therefore, caution should be taken in referencing previously reported data on the elasticity, yield strength, and crushing strength of individual sand particles. If possible, the experimental details such as the substrate material and its surface roughness should always be checked and compared.

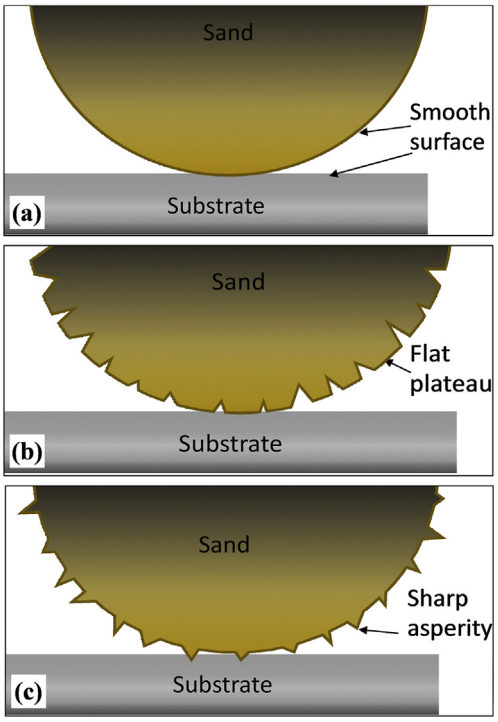

Fig. 10. Effect of surface roughness on the contact between the tested sand particle and substrate: (a) Smooth contact, where ideal Hertz contact occurs between smooth surfaces; (b) Frictional contact, where the rough surface of sand is characterized by flat plateaus; and (c) Frictional contact, where the rough surface of sand is characterized by sharp asperities.

As pointed out earlier, substrates made of materials with hardness smaller than that of the tested sand particles tend to yield an overestimated crushing strength (e.g. sometimes as high as 50%) and, if the local yielding in the particle-substrate contact is not considered, an underestimated yield strength and elastic modulus.

Fig. 9 compares the crushing strengths of the studied Ottawa sand with those published data for other sands (e.g. silica, quartz, and limestone). At the specific size (i.e. about 1 mm), Ottawa sand particles have the highest crushing strength, most likely due to their round or spherical shapes. Premature crushing or breakage may occur in angular or irregular particles, and hence these sands may possess lower crushing strength. A more in-depth comparison should further examine the substrate materials used to obtain these measurements before the data can be used correctly as inputs for DEM modeling.

5. Conclusions

This paper presents an experimental study to investigate the effects of different substrate materials on the evaluations of elastic, yielding, and crushing behaviors of individual sand particles. Although the tested material is Ottawa sand consisting of naturally occurring nearly spherical particles, similar phenomena and results can be expectedly extended to other sands with irregularly-shaped particles. Based on the above analysis and discussion, the following conclusions can be drawn:

(1) Despite the very small size range of the tested particles, their yielding and crushing strengths vary significantly. However, the statistical distributions of these properties can be well described by the Weibull law.

(2) Using Hertz elastic contact theory, the reduced modulus E_r that is related to the elastic properties of both the quartz particles and substrates varies with different substrates. As long as the elastic properties of the substrates are considered, the true Young's modulus of the sand particles can be determined and is hardly affected by the substrates.

(3) Both the apparent yielding and crushing strengths obtained by the substrates with a hardness less than that of the tested particles can be misleading. In fact, softer substrates lead to an underestimated apparent yield strength of harder sand particles, but an overestimated apparent crushing strength. In fact, the apparent crushing strengths of quartz particles obtained by softer aluminum alloy and stainless steel substrates increase by 50.4% and 36.4%, respectively.

(4) For individual sands' compression and crushing testing, particularly for the measurements of yielding and crushing strengths, the best practice is to use substrates with a hardness or yield strength greater than that of the tested particles.

Declaration of competing interest

The authors declare that they have no known competing financial interests or personal relationships that could have appeared to influence the work reported in this paper.

Acknowledgments

This work was partially supported by the National Natural Science Foundation of China (Grant Nos. 41372304 and 51679198), and China Scholarship Council Fellowship awarded to the first author. The authors are grateful to Dr. Yibing Deng of the University of Massachusetts Amherst for acquiring the optical images of sand particles.

References

Antonyuk, S., Heinrich, S., Tomas, J., Deen, N.G., van Buijtenen, M.S., Kuipers, J.A.M., 2010. Energy absorption during compression and impact of dry elastic-plastic spherical granules. Granul. Matter 12 (1), 15–47.

Antonyuk, S., Tomas, J., Heinrich, S., Mörl, L., 2005. Breakage behaviour of spherical granulates by compression. Chem. Eng. Sci. 60 (14), 4031–4044.

Bagherzadeh, K.A., Mirghasemi, A.A., Mohammadi, S., 2011. Numerical simulation of particle breakage of angular particles using combined DEM and FEM. Powder Technol. 205 (1–3), 15–29.

Bolton, M.D., 1986. The strength and dilatancy of sands. Geotechnique 36 (1), 65–78.

Brzesowsky, R.H., Spiers, C.J., Peach, C.J., Hangx, S.J.T., 2011. Failure behavior of single sand grains: theory versus experiment. J. Geophys. Res.: Solid Earth 116, B06205. http://dx.doi.org/10.1029/2010JB008120.

Cavarretta, I., Coop, M., O'Sullivan, C., 2010. The influence of particle characteristics on the behaviour of coarse grained soils. Geotechnique 60 (6), 413–423.

Cavarretta, I., O'Sullivan, C., Ibraim, E., Lings, M., Hamlin, S., Wood, D.M., 2012. Characterization of artificial spherical particles for DEM validation studies. Particuology 10 (2), 209–220.

Cheng, X.H., Ngan-Tillard, D.J.M., Haan, E.J.D., 2007. The causes of the high friction angle of Dutch organic soils. Eng. Geol. 93 (1–2), 31–44.

Cheng, Y.P., Nakata, Y., Bolton, M.D., 2003. Discrete element simulation of crushable soil. Geotechnique 53 (7), 633–641.

Cheshomi, A., Mousavi, E., Ahmadi-Sheshde, E., 2015. Evaluation of single particle loading test to estimate the uniaxial compressive strength of sandstone. J. Petrol. Sci. Eng. 135, 421–428.

Chester, J.S., Lenz, S.C., Chester, F.M., Lang, R.A., 2004. Mechanisms of compaction of quartz sand at diagenetic conditions. Earth Planet Sci. Lett. 220 (3–4), 435–451.

Chuhan, F.A., Kjeldstad, A., Bjørlykke, K., Høeg, K., 2003. Experimental compression of loose sands: relevance to porosity reduction during burial in sedimentary basins. Can. Geotech. J. 40, 995–1011.

Chuhan, F.A., Kjeldstad, A., Bjørlykke, K., Høeg, K., 2002. Porosity loss in sand by grain crushing – experimental evidence and relevance to reservoir quality. Mar. Petrol. Geol. 19 (1), 39–53.

Cil, M.B., Alshibli, K.A., 2012. 3D assessment of fracture of sand particles using discrete element method. Géotech. Lett. 2 (3), 161–166.

Cil, M.B., Alshibli, K.A., 2014. 3D evolution of sand fracture under 1D compression. Geotechnique 64 (5), 351–364.
Danzer, R., Supancic, P., Pascual, J., Lube, T., 2007. Fracture statistics of ceramics Weibull statistics and deviations from Weibull statistics. Eng. Fract. Mech. 74 (18), 2919–2932.
Daouadji, A., Hicher, P.Y., 2010. An enhanced constitutive model for crushable granular materials. Int. J. Numer. Anal. Methods GeoMech. 34 (6), 555–580.
Druckrey, A.M., Alshibli, K.A., Al-Raoush, R.I., 2016. 3D characterization of sand particle-to-particle contact and morphology. Comput. Geotech. 74, 26–35.
Du, J.T., Hu, L.M., Meegoda, J.N., Zhang, G.P., 2018. Shale softening: observations, phenomenological behavior, and mechanisms. Appl. Clay Sci. 161, 290–300.
Einav, I., 2007a. Breakage mechanics – Part I: theory. J. Mech. Phys. Solid. 55 (6), 1274–1297.
Einav, I., 2007b. Breakage mechanics – Part II: modelling granular materials. J. Mech. Phys. Solid. 55 (6), 1298–1320.
Fischer-Cripps, A.C., 2011. Nanoindentation. Springer-Verlag Inc., New York.
Haki, A., El Hadi, M.A., Bouhafid, A., 2017. Assessment of the pyrolysis, combustion and fractal dimension of fragmented oil shale particles. Powder Technol. 318, 569–588.
Hibare, S., Sivanathan, R., Nadakatti, S., 2011. Behaviour of soft granules under compression: effect of reactive and non-reactive nature of the binder on granule properties. Powder Technol. 210 (3), 241–247.
Hiramatsu, Y., Oka, Y., 1966. Determination of the tensile strength of rock by a compression test of an irregular test piece. Int. J. Rock Mech. Min. Sci. Geomech. Abstr. 3 (2), 89–90.
Jaeger, J.C., 1967. Failure of rocks under tensile conditions. Int. J. Rock Mech. Min. Sci. Geomech. Abstr. 4 (2), 219–227.
Jayatilaka, A.S., Trustrum, K., 1977. Statistical approach to brittle fracture. J. Mater. Sci. 12, 1426–1430.
Johnson, K.L., 1985. Contact Mechanics. Cambridge University Press, Cambridge, UK.
Karner, S.L., Chester, J.S., Chester, F.M., Kronenberg, A.K., Hajash, A., 2005. Laboratory deformation of granular quartz sand: implications for the burial of clastic rocks. AAPG (Am. Assoc. Pet. Geol.) Bull. 89 (5), 603–625.
Kikumoto, M., Wood, D.M., Russell, A., 2010. Particle crushing and deformation behaviour. Soils Found. 50 (4), 547–563.
Kwag, J.M., Ochiai, H., Yasufuku, N., 1999. Yielding stress characteristics of carbonate sand in relation to individual particle fragmentation strength. In: Engineering for Calcareous Sediments. A.A. Balkema, pp. 79–86.
Lee, D.M., 1992. The Angles of Friction of Granular Fills. PhD Thesis. Department of Civil Engineering, University of Cambridge, Cambridge, UK.
Luscher, W.G., Hellmann, J.R., Segall, A.E., Shelleman, D.L., Scheetz, B.E., 2007. A critical review of the diametral compression method for determining the tensile strength of spherical aggregates. J. Test. Eval. 35 (6), 624–629.
McDowell, G.R., Bolton, M.D., Robertson, D., 1996. The fractal crushing of granular materials. J. Mech. Phys. Solid. 44 (12), 2079–2101.
McDowell, G.R., Harireche, O., 2002. Discrete element modelling of yielding and normal compression of sand. Geotechnique 52 (4), 299–304.
Menčík, J., Swain, M.V., 1997. Design of contact loaded coated components using data from depth sensing microindentation tests. Surf. Eng. 13 (6), 498–504.
Müller, P., Antonyuk, S., Tomas, J., 2011. Influence of moisture content on the compression behavior of granules. Chem. Eng. Technol. 34 (9), 1543–1550.
Müller, P., Seeger, M., Tomas, J., 2013. Compression and breakage behavior of γ-Al_2O_3 granules. Powder Technol. 237, 125–133.
Nakata, Y., Kato, Y., Hyodo, M., Hyde, A.F.L., Murata, H., 2001. One-dimensional compression behaviour of uniformly graded sand related to single particle crushing strength. Soils Found. 41 (2), 39–51.
Pejchal, V., Žagar, G., Charvet, R., Dénéréaz, C., Mortensen, A., 2017. Compression testing spherical particles for strength: theory of the meridian crack test and implementation for microscopic fused quartz. J. Mech. Phys. Solid. 99, 70–92.
Peng, H.H., Lin, C.K., Chung, Y.C., 2014. Effects of particle stiffness on mechanical response of granular solid under confined compression. Procedia Eng. 79, 143–152.
Pestana, J.M., Whittle, A.J., 1995. Compression model for cohesionless soils. Geotechnique 45 (4), 611–631.
Pharr, G.M., Oliver, W.C., Brotzen, F.R., 1992. On the generality of the relationship among contact stiffness, contact area, and elastic modulus during indentation. J. Mater. Res. 7 (3), 613–617.
Qian, G., Lei, W.S., Yu, Z., Berto, F., 2019. Statistical size scaling of breakage strength of irregularly-shaped particles. Theor. Appl. Fract. Mech. 102, 51–58.
Rahmanian, N., Ghadiri, M., Jia, X., Stepanek, F., 2009. Characterisation of granule structure and strength made in a high shear granulator. Powder Technol. 192 (2), 184–194.
Roscoe, K.H., Burland, J.B., 1968. On the generalised stress-strain behaviour of "wet" clay. In: Heyman, J., Leckie, F.A. (Eds.), Engineering Plasticity. Cambridge University Press, Cambridge, UK, pp. 535–609.
Roscoe, K.H., Schofield, A.N., Wroth, C.P., 1958. On the yielding of soils. Geotechnique 8 (1), 22–53.
Santamarina, J.C., Cho, G.C., 2004. Soil behaviour: the role of particle shape. In: Advances in Geotechnical Engineering: the Skempton Conference. ICE Publishing, pp. 604–617.
Shipway, P.H., Hutchings, I.M., 1993a. Fracture of brittle spheres under compression and impact loading. I. Elastic stress distributions. Philos. Mag. A 67 (6), 1389–1404.
Shipway, P.H., Hutchings, I.M., 1993b. Fracture of brittle spheres under compression and impact loading. II. Results for lead-glass and sapphire spheres. Philos. Mag. A 67 (6), 1405–1421.
Song, J.L., Sun, Q.S., Luo, S.M., Arwade, S.R., Gerasimidis, S., Guo, Y., Zhang, G.P., 2018. Compression behavior of individual thin-walled metallic hollow spheres with patterned distributions of microporosity. Mater. Sci. Eng. A 734, 453–475.
Song, J.L., Sun, Q.S., Yang, Z.N., Luo, S.M., Xiao, X., Arwade, S.R., Yi, G., Zhang, G.P., 2017. Effects of microporosity on the elasticity and yielding of thin-walled metallic hollow spheres. Mater. Sci. Eng. A 688, 134–145.
Todisco, M.C., Wang, W., Coop, M.R., Senetakis, K., 2017. Multiple contact compression tests on sand particles. Soils Found. 57, 126–140.
Wang, Y.D., Dan, W.J., Xu, Y.F., Xi, Y., 2015. Fractal and morphological characteristics of single marble particle crushing in uniaxial compression tests. Adv.Mater. Sci. Eng. http://dx.doi.org/10.1155/2015/537692.
Weibull, W., 1951. A statistical distribution function of wide applicability. ASME J. Appl. Mech. 18 (3), 293–297.
Wenzel, V., Nirschl, H., 2015. Validation of an inline particle probe in a high-shear mixer for particle size determination. Powder Technol. 269, 178–184.
Wu, S.Z., Chau, K.T., Yu, T.X., 2004. Crushing and fragmentation of brittle spheres under double impact test. Powder Technol. 143–144, 41–55.
Yamamuro, J.A., Bopp, P.A., Lade, P.V., 1996. One-dimensional compression of sands at high pressures. J. Geotech. Eng. 122 (2), 147–154.
Yoshimoto, N., Hyodo, M., Nakata, Y., Orense, R.P., Hongo, T., Ohnaka, A., 2012. Evaluation of shear strength and mechanical properties of granulated coal ash based on single particle strength. Soils Found. 52 (2), 321–334.
Zhang, G.P., Yin, H., Degroot, D.J., 2013. Thixotropism of micron-sized saltwater clay flocs. Géotech. Lett. 3 (4), 162–165.
Zhang, J., Wong, T., Davis, D.M., 1990. Micromechanics of pressure-induced grain crushing in porous rocks. J. Geophys. Res.: Solid Earth 95 (B1), 341–352.

Chunlong Liu obtained his BSc degree in Geotechnical and Underground Engineering from Heilongjiang Institute of Technology, China, in 2012, and his MSc degree from Institute of Geotechnical Engineering at Xi'an University of Technology, China, in 2015. He is now a PhD candidate majoring in Geotechnical Engineering at Xi'an University of Technology. In 2018, he was awarded by China Scholarship Council Fellowship and learned at University of Massachusetts Amherst (UMASS Amherst) as a Visiting Student where he worked in Civil and Environmental Engineering research in contact mechanics of particles and interaction between clay mineral and organic polymer. His research currently focuses on geotechnical engineering and testing technology and theory.